

S. KUT

ISSN 0543-5846

METABK 49(4) 295-299 (2010)

UDC – UDK 669.14-418:539.37:620.17=111

## A SIMPLE METHOD TO DETERMINE DUCTILE FRACTURE STRAIN IN A TENSILE TEST OF PLANE SPECIMEN'S

Received – Prispjelo: 2009-11-05

Accepted – Prihvaćeno: 2009-12-18

Original Scientific Paper – Izvorni znanstveni rad

The ultimate ductile fracture strain determination method for the specimen of circular cross-section has been presented by FEM method. The state of stress in individual locations of tensile tested specimen in successive process phases has been determined unequivocally with the stress triaxiality  $k$ . It has been demonstrated that the plane specimen's fracture strain value in the fracture location varies and depends on the state of stress, which is present in the final specimen's tension phase. The ductile fracture strain values in various fracture locations for steel, copper and aluminum specimen have been experimentally determined and compared. The simple and practical method to determine this strain has been proposed.

*Key words:* tensile test, ductile fracture strain, stress triaxiality, finite element method (FEM)

**Jednostavna metoda određivanja plastičnoga prijeloma i čvrstoće plošnih uzoraka.** U članku je data metoda proračuna određivanja plastičnoga loma uzoraka s okruglim prijesekom sa MKE metodom. Stanje naprezanja u pojedinačnim mjestima vlačnog pokusnog uzorka u pojedinim fazama procesa su bile određene koeficijentom troosnog naprezanja  $k$ . Dokazano je, vrijednosti naprezanja pri lomu plošnih uzoraka u oblasti prijeloma se mijenjaju u ovisnosti od stanja naprezanja koje je pokazano u završnoj fazi vučenog uzorka. Vrijednosti deformacije pri plastičnom razaranju u raznim mjestima prijeloma za čelik, bakar i aluminij su bile eksperimentalne proračunate i uspoređene. Određena je jednostavna i praktička metoda pri proračunu tih deformacija.

*Ključne riječi:* vlak, plastično razaranje, troosno stanje naprezanja, metoda konačnih elemenata (MKE)

### INTRODUCTION

In several practical cases, the ultimate ductile fracture strain determined with tensile test is accepted as a material plasticity measure [1]. In this case, the plasticity has to be defined as an ability of a material to accommodate high permanent strains until fracture appears where this strain reaches certain value called ultimate fracture strain  $\varepsilon_p$ . The strain value until fracture depends not only on the material type, but also on other several factors, as: strain speed, strain history, material starting structure, temperature, specimen geometry, etc. It is impossible to account for all factors in a single mathematical description, due to a complexity of phenomena and an insufficient state of the art, mainly for phenomena present during a plastic strain. Several experiments [2-5] have demonstrated that the material fracture process strongly depends on the hydrostatic stress. This conclusion has been independently induced based on experiments [6-8].

Recently, several different fracture criteria, including the state of hydrostatic stress, have been developed [8-10]. However, the practical application of above cri-

teria to forecast the fracture during the metal forming process has been feasible thanks the numerical computing methods, which enable to determine the material's state of stress during the plastic forming process. Currently, the ductile fracture criteria are commonly used when simulating various plastic processing processes [10-13]. However, the practical application of the criteria requires the experimental determination of the ductile fracture strain  $\varepsilon_p$  value for a given material. This strain is usually determined based on the tensile test, but the determination method indeed is not so obvious, and in several cases even doubtful.

In most cases, the tensile test is performed against circular or rectangular cross-section specimens. Considering that the ductile fracture strain  $\varepsilon_p$  around the fracture zone equals the equivalent strain  $\varepsilon_z$  in this zone, it can be calculated using the equation:

$$\varepsilon_p = \varepsilon_z = \sqrt{\frac{2}{3}} \cdot \sqrt{\varepsilon_1^2 + \varepsilon_2^2 + \varepsilon_3^2} \quad (1)$$

For circular cross-section specimen (Figure 1a), the strain components in direction 1 and 2 are calculated using the equation:

$$\varepsilon_1 = \varepsilon_2 = \varepsilon = \ln \frac{d_1}{d_0} \quad (2)$$

S. Kut, Faculty of Mechanical Engineering and Aeronautics, Rzeszów University of Technology, Rzeszów, Poland

The strain component in direction 3 is calculated using the constant volume condition:

$$\varepsilon_1 + \varepsilon_2 + \varepsilon_3 = 0 \Rightarrow \varepsilon_3 = -2\varepsilon \quad (3)$$

If (2) and (3) are substituted to (1) and transformed, the equation to determine the ductile fracture strain  $\varepsilon_p$  for circular cross-section specimen is achieved.

$$\varepsilon_p = 2 \ln\left(\frac{d_1}{d_0}\right) \quad (4)$$

If a tensile tested specimen is plane (Figure 1b), the strain components in directions 1 and 2 are different and may be calculated using the equation:

$$\varepsilon_1 = \ln\left(\frac{b_1}{b_0}\right) \quad (5)$$

$$\varepsilon_2 = \ln\left(\frac{g_1}{g_0}\right) \quad (6)$$

The strain component in direction 3 is calculated using the equation:

$$\varepsilon_1 + \varepsilon_2 + \varepsilon_3 = 0 \Rightarrow \varepsilon_3 = -(\varepsilon_1 + \varepsilon_2) \quad (7)$$

If (5), (6) and (7) are substituted to (1), the equation to determine the ductile fracture strain  $\varepsilon_p$  for rectangular cross-section specimen is achieved:

$$\varepsilon_p = \sqrt{\frac{2}{3} \cdot \sqrt{\varepsilon_1^2 + \varepsilon_2^2 + [-(\varepsilon_1 + \varepsilon_2)]^2}} \quad (8)$$

The equation (8) has been derived provided that the specimen's cross-section shape is not changed after the strain. Actually, the specimen's cross-section shape after the tensile failure differs significantly from the starting shape (Figure 2a). After the tensile failure, the plane specimen's cross-section has a shape of a saddle (Figure 2b), and it means that the ductile fracture strain value is not identical within the cross-section, but varies significantly. That's why the calculation of the ductile fracture

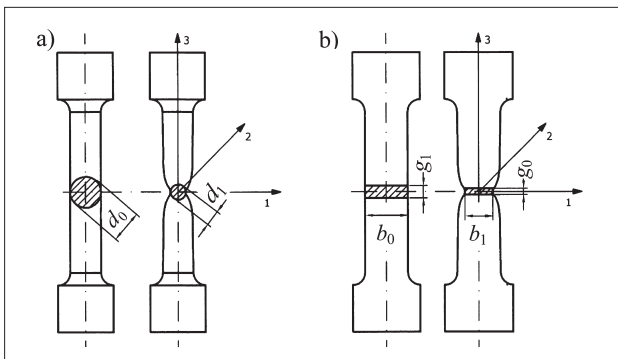


Figure 1 Typical tensile specimens: a) a round specimen, b) a flat specimen

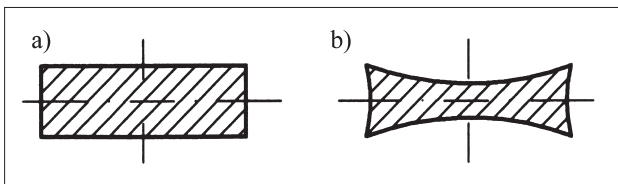


Figure 2 Cross-sectional area in the neck at fracture: a) before fracture, b) after fracture

strain  $\varepsilon_p$  for plane specimen is not so obvious, as for the circular cross-section specimen.

The lack of reference data how to proceed in this case has been a basis to perform the experiments, in order to develop the method to specify the ductile fracture strain  $\varepsilon_p$  for rectangular cross-section specimens.

## EXPERIMENTAL WORK

The static tensile test has been performed using UTS 100 tensile testing machine. The plane sheet metal specimens have been tested made of the following material: steel, copper, and aluminum 5 251. The mechanical characteristics and the strain hardening curve parameters for tested materials, achieved based on the tensile test, have been presented in Table 1. In order to determine material constants  $K$  and  $n$ , the specimen elongation has been measured using the extensometer along the section  $l_0 = 80$  mm. Then the strain hardening curve  $\sigma_p = f(\varepsilon)$  has been plotted for the points below maximum tension force. The stress  $\sigma_p$  for individual strain hardening curve points has been calculated as the ratio of the force to the variable specimen cross-section, calculated based on the constant volume condition. The logarithmic strain for individual strain hardening curve points has been calculated from the equation  $\varepsilon = \ln(l/l_0)$ , where:  $l_0 = 80$  mm,  $l$  – the length of section after specimen elongation. The strain hardening curve points calculated this way have been approximated with an equation  $\sigma_p = K\varepsilon^n$ . The measuring bases to indicate the measuring zone have been marked on the specimen surface. L, P – Lateral, S – Middle (Figure 3). The zone width and specimen thickness have been measured in these locations before and after the specimen tensile failure. The geometrical values have been measured using the toolmaker's microscope with an accuracy of 0,01 mm. The average specimen thickness  $g_1$  after the tensile failure within individual areas (L, P, and S, C) has been determined as follows:

- 1) the specimen thickness has been measured after the tensile failure in examined areas, with an interval of approx. 0,5 mm on specimen width,
- 2) thickness  $g_1$  has been calculated as an arithmetical mean of measured thickness values within individual areas.

The measured values of geometrical parameters in individual locations before and after the specimen ten-

Table 1 Mechanical properties of materials tested

Material	Yield stress $R_e$ /MPa	Ultimate strength $R_m$ /MPa	Strain hardening coefficient	Strain hardening exponent
			$K$ /MPa	$n$
steel	399	447	591	0,072
copper	97	217	389	0,262
aluminium	65	175	378	0,31

Table 2 Specimen's geometry and average strain values in analyzed regions

Material	Designation of parameter		Measuring zones		
			L, P lateral	S middle	C total
Steel	values of geometrical parameters [mm]	$g_0$	3,55	3,55	3,55
		$b_0$	2,1	2	14,92
		$g_1$	2,34	1,7	2,2
		$b_1$	1,47	1,56	10,97
	plastic strain	$\varepsilon_1$	-0,357	-0,248	-0,307
		$\varepsilon_2$	-0,417	-0,736	-0,564
		$\varepsilon_p$	<b>0,774</b>	<b>1,024</b>	<b>0,884</b>
Copper	values of geometrical parameters [mm]	$g_0$	3,55	3,55	3,55
		$b_0$	2,1	2,1	14,85
		$g_1$	1,27	0,98	1,12
		$b_1$	1,51	1,48	10,05
	plastic strain	$\varepsilon_1$	-0,32	-0,35	-0,39
		$\varepsilon_2$	-1,028	-1,278	-1,154
		$\varepsilon_p$	<b>1,416</b>	<b>1,724</b>	<b>1,606</b>
Aluminium	values of geometrical parameters [mm]	$g_0$	3,55	3,55	3,55
		$b_0$	2,1	2,25	14,78
		$g_1$	2,1	1,75	1,95
		$b_1$	1,81	1,93	11,75
	plastic strain	$\varepsilon_1$	-0,148	-0,153	-0,229
		$\varepsilon_2$	-0,525	-0,707	-0,599
		$\varepsilon_p$	<b>0,707</b>	<b>0,918</b>	<b>0,855</b>

sile failure, for individual materials have been stated in Table 2. Then for all measured zones, the strain value  $\varepsilon_1$  and strain value  $\varepsilon_2$  have been calculated using (5) and (6), and then the ductile fracture strain values in an individual zones have been calculated using (8) (Table 2).

The analysis of the fracture strain value  $\varepsilon_p$  for individual materials demonstrates that, for all cases, the highest strain appears in the middle part of specimen, and the lowest in the lateral part. The experiments performed show that the more plastic material is (in this case - copper), the higher fracture strain value  $\varepsilon_p$  difference. For aluminum and copper specimen, both the strain  $\varepsilon_1$  in direction 1 (specimen width) and the strain  $\varepsilon_2$  in direction 2 (specimen thickness) achieve the highest value in zone S, its middle part. Whereas for the steel specimen, the highest strain  $\varepsilon_2$  appears in direction 2 (specimen thickness) in zone S, and in direction 1 (specimen width) strain  $\varepsilon_1$  is slightly lower than in its middle part (Table 2).

It is also supposed that the differences between strains in the middle and lateral part of the specimen will increase as the specimen width is increased. The mean strain value measured for an entire specimen is inaccurate and depends mainly on its geometry. The following question arises: where the fracture strain for the plane specimens should be measured?

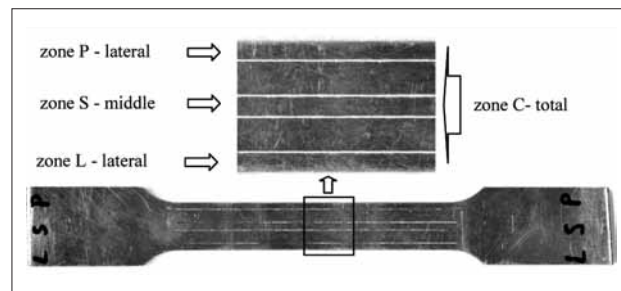


Figure 3 Tensile specimen with marked control lines

## FEM NUMERICAL SIMULATION

To answer the question as referred to the above, the steel specimen tension process numerical simulation has been performed using MSC Marc Mentat software, which enables solving non-linear and contact problems. FEM simulation's geometrical model has been created based on the experimental model. The purpose of the numerical simulation in this case is neither detailed analysis of stresses and strains nor determining their values. The purpose of the simulation is to indicate the area, where the state of stress on the tensioned specimen is the closest to uniaxial tension, within an entire strain range up to specimen tensile failure. Therefore the specimen tension process has been analyzed in the plane stress condition. The elastic-plastic material model with non-linear strain hardening has been adopted, described by the following equation [14]:

$$\sigma = \begin{cases} E \cdot \varepsilon & (\sigma \leq \sigma_0) \\ K \cdot \varepsilon^n & (\sigma > \sigma_0) \end{cases} \quad (9)$$

The material parameters for elastic strain have been as follows:  $E = 210000$  MPa,  $\nu = 0,3$ . The strain hardening parameters  $K, n$  are presented in Table 1. In order to create FEM grid of deformable sheet metal, Class 4 Type 3 elements has been used – plane-stress quadrilateral [15]. The start point of necking has been determined based on Hill's equation in form of [16]:

$$\varepsilon^* = \frac{n}{(1 + \rho)} \quad (10)$$

where:  $\varepsilon^*$  - critical strain for the onset of local necking,  $\rho = \varepsilon_3 / \varepsilon_1$ ,  $n$  - strain hardening exponent.

The tension simulations have been performed for an entire specimen, placed in the measuring area of an extensometer (II) holding the gripping area of the specimen, right at the tensile testing machine grips. Such a purposeful placement of the extensometer (II) enabled the introduction of the movement boundary condition for the specimen modeled as in the experiment. This also enabled eliminating the machine structure susceptibility errors. The boundary condition has been also introduced for nodes placed at the ends of modeled specimen in the measuring area of an extensometer (II). The node movements towards the specimen axis have been forced in the boundary condition. The node movement perpendicularly towards the specimen has been disallowed.

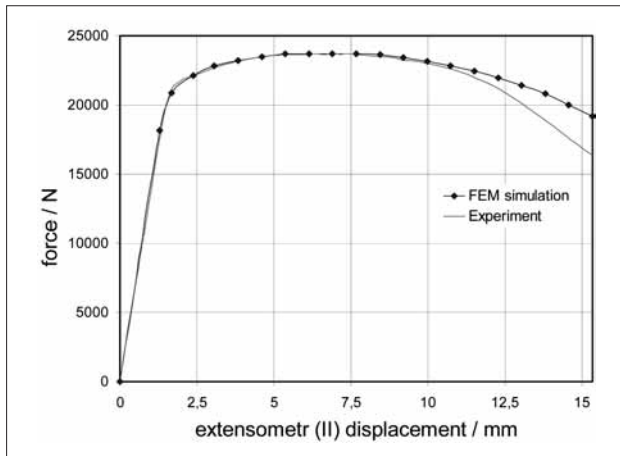


Figure 4 Comparison of the tensile force-experimental and numerical results (steel specimen)

Due to such an assumed boundary condition, the local necking appears exactly halfway the length of tensioned specimen.

The tension simulation has been performed until specimen tensile failure, and it corresponds to extensometer (II) displacement, which was 15,33 mm for the steel specimen. The tensile force curves have been prepared and compared (Figure 4) in order to validate the FEM simulation. The limit value of ductile fracture strain depends on the present state of stress. In the mechanical & mathematical modeling approach, non-dimensional stress triaxiality  $k = \sigma_m / \sigma_H$ , where  $\sigma_m$  is a mean normal stress,  $\sigma_H$  is an equivalent stress, is the very important parameter, which unequivocally specifies the plane state of stress (Figure 5). If this factor is known, it is possible to determine the state of stress in any point of strained object, e.g.: if  $k = 0$  – this is a simple shear (Figure 5.c),  $k = 0,66$  – it is a biaxial regular tension (Figure 5.e),  $k = -0,33$  – it is an uniaxial compression (Figure 5.b), etc.

In considered case we determine the strain for the tensile test, so that  $k$  factor value is 0,33. As seen in FEM calculations, the uniaxial state of stress is present in an initial tension phase and lasts until the neck is created, and then once  $R_m$  limit is exceeded, the states of stress in individual zones differ significantly (Figure 6).

The state of stress in the lateral zone  $L$  changes slightly in the biaxial tension direction, reaching  $k = 0,36$  in its final phase. Whereas the state of stress in the middle zone  $S$  changes significantly in the simple shear direction, reaching  $k = 0,106$  in its final phase.

The state of stress factor  $k$  distribution in the initial and final phase of the specimen tensile test has been presented on Figure 7. The  $k$  factor value is explicitly different in the middle and lateral part of the specimen under test.

CONCLUSIONS

1. The experiments performed show that the fracture strain in the tensile test for plane specimen

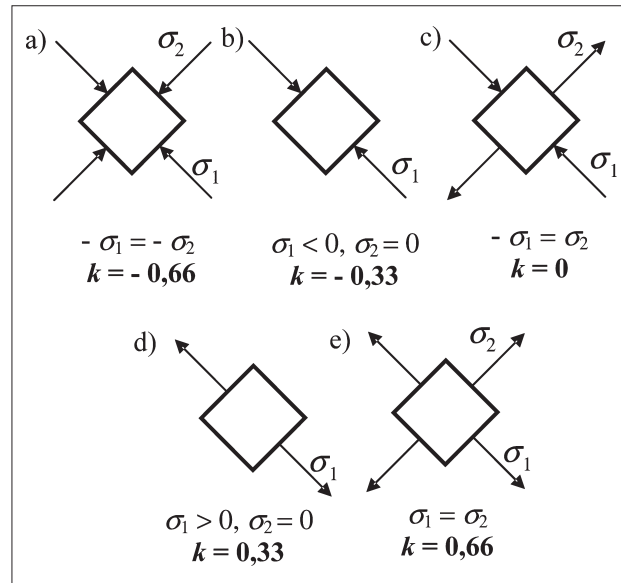


Figure 5 The  $k$  factor values for an individual plane stress cases: a) biaxial compression, b) uniaxial compression, c) simple shear, d) uniaxial tension, e) biaxial tension

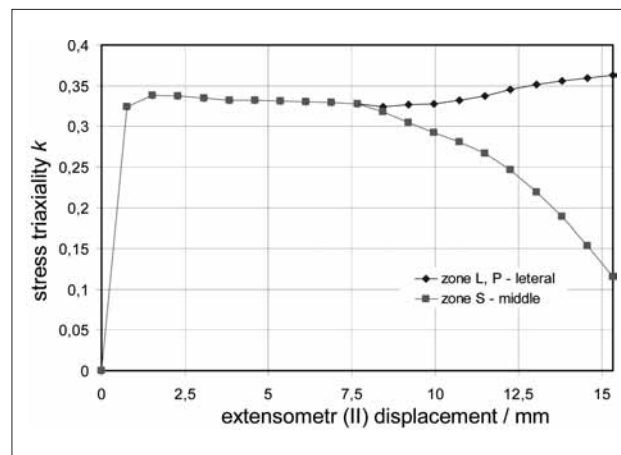


Figure 6 Comparison of stress triaxiality in different specimen zone: L, P – lateral, S - middle

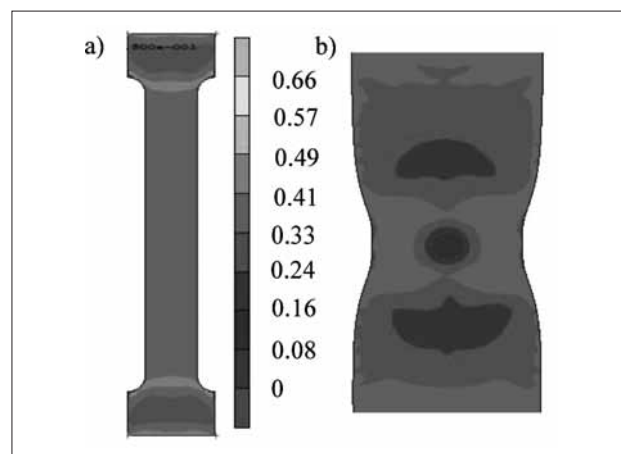


Figure 7 Distribution of stress triaxiality  $k$ : a) initial phase of tensile test (3-item), b) final phase of tensile test (20-item)

must be determined in  $L$  or  $P$  zone, as the state of stress in these zones is the closest to the uniaxial tension for all tensile test.

2. The calculation of the ductile fracture strain for an entire cross-section  $C$  is highly inaccurate and the error mostly depends on the specimen dimensions.
3. The presented method of the ductile fracture strain determination is simple and can be performed during the conventional tensile test, once the base line is marked on the specimen surface.

## REFERENCES

- [1] Czichos, H., Saito, T., Smith L.: Springer Handbook of Materials Measurement Methods. Springer-Verlag New York, 2006, pp. 302-307.
- [2] Bao, Y., Wierzbicki, T.: On fracture locus in the equivalent strain and stress triaxiality space. *Int. J. Mech. Sci.* 46 (2004), 81-98.
- [3] Mohr, D., Henn, S.: Calibration of stress-triaxiality dependent crack formation criteria: A new hybrid experimental-numerical method. *Exp.Mech.* 47 (2007), 805-820.
- [4] Oh, C.-K., et al.: Development of stress-modified fracture strain for ductile failure of API X65 steel, *Int. J. Fract.* 143 (2007), 119-133.
- [5] Kim, J., et al.: Modeling of void growth in ductile solids: Modeling of void growth in ductile solids: effects of stress triaxiality and initial porosity. *Eng. Fract. Mech.* 71 (2004), 379-400.
- [6] Bao, Y.: Dependence of ductile crack formation in tensile tests on stress triaxiality, stress and strain ratios. *Eng. Fract. Mech.* 72 (2005), 505-522.
- [7] Zhu, H., et al.: Investigation of fracture mechanism of 6063 aluminum alloy under different stress states. *Int. J. Fract.* 146 (2007), 159-172.
- [8] Zhao, Z., et al.: An improved ductile fracture criterion for fine-blanking process. *J. Shanghai Univ. (Sci.)*, 13 (2008) 6, 702-706.
- [9] Oyane, M., et al.: Criteria for ductile fracture and their applications. *J. Mech. Working Techn.* 4 (1980), 65-81.
- [10] Hambli, R., Reszka, M.: Fracture criteria identification using an inverse technique method and blanking experiment. *Int. J. Mech. Sci.* 44 (2002), 1349-1361.
- [11] KUT, S.: The method of ductile fracture modeling and predicting the shape of blanks. *Progressive Technologies and Materials. OWPRz, Rzeszów*, 2007, 15-25.
- [12] Thipprakmas, S., et al.: An investigation of step taper-shaped punch in piercing process using finite element method. *J. Mat. Proc. Techn.* 197 (2008), 132-139.
- [13] Yu, S., et al.: Ductile fracture modeling of initiation and propagation in sheet-metal blanking processes, *J. Mat. Proc. Techn.* 187-188 (2007), 169-172.
- [14] Chen, W.F., Han D. J.: *Plasticity for Structural Engineers*. Springer-Verlag New York, 1988, 12.
- [15] MSC Software, MSC.Marc Volume B, Element Library, Version 2007.
- [16] MSC Software, MSC.Marc Volume A, Theory and User Information, Version 2007.

**Note:** The responsible translator English language is G. Rębisz, Rzeszów, Poland.